Single-layer dual germanene phases on Ag(111)

Chung-Huang Lin,[1,2] Angus Huang,[1] Woei Wu Pai,[2,3,*] Wei-Chuan Chen,[1] Ting-Yu Chen,[1] Tay-Rong Chang,[1] Ryu Yukawa,[4] Cheng-Maw Cheng,[5] Chung-Yu Mou,[1] Iwao Matsuda,[4] T.-C. Chiang,[3,6] H.-T. Jeng,[1,7,†] and S.-J. Tang[1,5,‡]

[1]*Department of Physics, National Tsing Hua University, Hsinchu 30013, Taiwan*
[2]*Center for Condensed Matter Sciences, National Taiwan University, Taipei 106, Taiwan*
[3]*Department of Physics, National Taiwan University, Taipei 106, Taiwan*
[4]*Institute for Solid State Physics, the University of Tokyo, 5-1-5, Kashiwanoha, Kashiwa, Chiba 277–8581, Japan*
[5]*National Synchrotron Radiation Research Center (NSRRC), Hsinchu 30076, Taiwan*
[6]*Department of Physics, University of Illinois at Urbana-Champaign, 1110 West Green Street, Urbana, Illinois 61801-3080, USA*
[7]*Institute of Physics, Academia Sinica, Taipei 11529, Taiwan*

(Received 8 May 2017; revised manuscript received 17 January 2018; published 9 February 2018)

Two-dimensional (2D) honeycomb lattices beyond graphene promise new physical properties such as quantum spin Hall effect. While there have been claims of growth of such lattices (silicene, germanene, stanene), their existence needs further support and their preparation and characterization remain a difficult challenge. Our findings suggest that two distinct phases associated with germanene, the analog of graphene made of germanium (Ge) instead of carbon, can be grown on Ag(111) as observed by scanning tunneling microscopy, low-energy electron diffraction, and angle-resolved photoemission spectroscopy. One such germanene exhibits an atom-resolved alternatively buckled full honeycomb lattice, which is tensile strained and partially commensurate with the substrate to form a striped phase (SP). The other, a quasifreestanding phase (QP), is also consistent with a honeycomb lattice with a lattice constant incommensurate with the substrate but very close to the theoretical value for freestanding germanene. The SP, with a lower atomic density, can be driven into the QP and coexist with the QP by additional Ge deposition. Band mapping and first-principles calculations with proposed SP and QP models reveal an interface state exists only in the SP but the characteristic σ band of freestanding germanene emerges only in the QP—this leads to an important conclusion that adlayer-substrate commensurability plays a key role to affect the electronic structure of germanene. The evolution of the dual germanene phases manifests the competitive formation of Ge-Ge covalent and Ge-Ag interfacial bonds.

DOI: 10.1103/PhysRevMaterials.2.024003

I. INTRODUCTION

The discovery of graphene [1] has spurred great interest in the exploration of novel 2D materials including graphene's siblings made of other group IV elements. Specifically, silicene, germanene, and stanene, made of Si, Ge, and Sn, respectively, are expected to form a low-buckled, instead of flat, honeycomb lattice because of a stronger sp^3 bonding character. Their stronger spin-orbital coupling leads to a sizable band gap, as opposed to the nearly zero gap in graphene, making them well suited for a variety of device applications. Furthermore, all of them are 2D topological insulators with a quantum spin Hall response [2]. Silicon and germanium are mainstream semiconductor materials; any new form of Si and Ge would likely bear technological importance.

Synthesis and characterization of silicene [3–10], germanene [11–18], and even stanene [19] have been reported, but controversies remain. For example, one early angle-resolved photoemission spectroscopy (ARPES) observation [3] of a Dirac cone feature in silicene prepared on Ag(111) was later identified as the projected Ag bulk band edge [4]. Several ARPES studies of multilayer silicene revealed a Dirac cone feature, but it was located at the wrong place in the surface Brillouin zone (SBZ) [7]. The reported $(\sqrt{3} \times \sqrt{3})$ multilayer silicene might in fact be bulk silicon with a Ag adlayer [6–10]. Germanene was less studied than silicene but it has been reported to grow on Ge_2Pt [13], Pt(111) [14], Al(111) [15], Au(111) [16,17], and MoS_2 [18]. However, few ARPES and scanning tunneling microscopy (STM) experiments thus far for silicene, germanene, and stanene have yielded strong evidence for the characteristic low-buckled honeycomb lattice or the corresponding electronic structure [3,17]. The atomic coverage and the species imaged by STM were also questioned [6]. Consequently, conclusive experimental results and consistent theoretical analysis on the geometric and electronic structures of group IV honeycomb lattices beyond graphene remain elusive.

A better understanding of the growth of 2D-Xenes (i.e., silicene, germanene, stanene) is needed to further probe their important structure-property correlations. It has been suggested that a commensurate substrate would promote the epitaxial growth of Xenes [20] but the effects of adlayer-substrate commensurability have not been explored. Although adequate interaction with the substrate is expected to promote the growth of a 2D atomic layer, optimal lattice match may instead generate interfacial electronic structures deteriorating the intrinsic ones. Here we report evidence that two buckled

*wpai@ntu.edu.tw
†jeng@phys.nthu.edu.tw
‡sjtang@phys.nthu.edu.tw

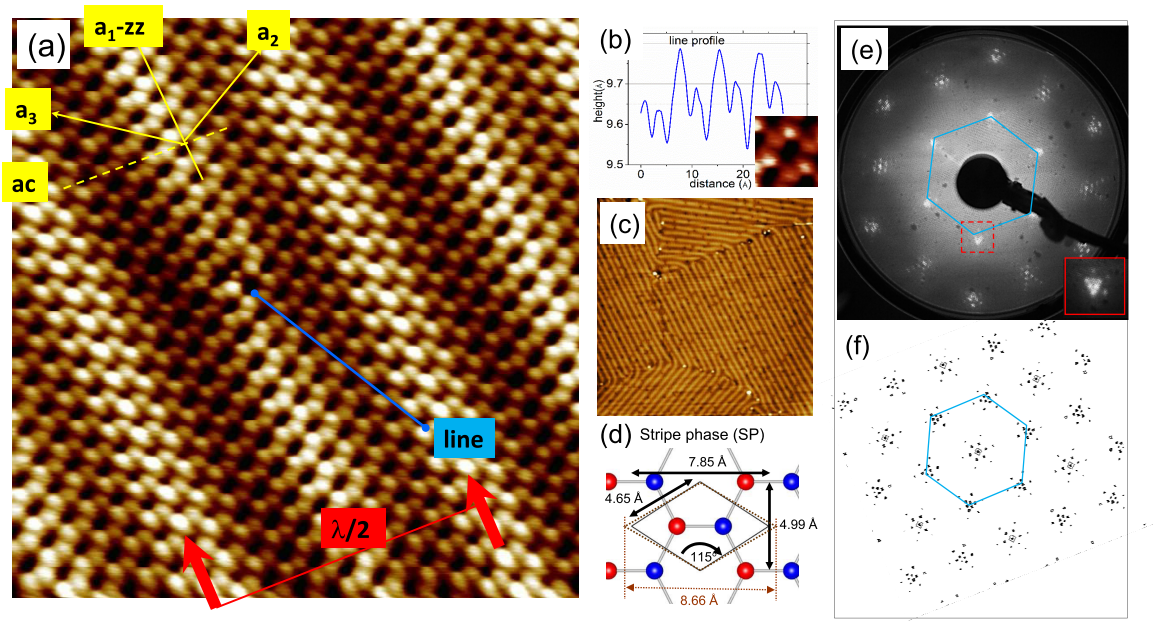

FIG. 1. "Striped phase" germanene. (a) Atomic view of a germanene lattice grown on Ag(111) (image size, tunneling sample bias, and current: 8 × 8 nm, 0.29 V, and 0.95 nA). Note that all Ge atoms are resolved and show an alternating up-and-down low buckle pattern. This SP germanene is commensurate with the Ag lattice in the stripe direction (i.e., germanene lattice zigzag direction $\mathbf{a_1}$**-zz**). The germanene lattice constant along the armchair (**ac**) direction is compressed, leading to smaller lattice spacings (cf. in the $\mathbf{a_1}$ direction) along $\mathbf{a_2}$ and $\mathbf{a_3}$. The incommensurability along **ac** leads to stripe features. (b) A line profile [line in (a)] shows a buckling height ∼0.1 Å. The inset shows a magnified view of a buckled hexagon. (c) Coexistence of three orientation striped-phase domains separated by 120° (image size, tunneling sample bias, and current: 60 × 60 nm, −412 mV, and 0.91 nA). (d) Top view of the striped phase model. Dashed line rhombus indicates a $(\sqrt{3} \times \sqrt{3})R30°$ cell. (e) LEED diffraction pattern at 75-eV beam energy. Note that all LEED spots consist of satellite features (e.g., see inset red box). (f) Simulation of the LEED pattern of (e). See content for details.

honeycomb germanene phases, with distinct adlayer-substrate commensurability, can be prepared on Ag(111). The geometric and electronic structures of these two phases, and their evolution, were measured by low-energy electron diffraction (LEED), STM, ARPES and were corroborated with detailed first-principles calculations. The dual germanene phases reveal that adlayer-substrate commensurability renormalizes the intrinsic electronic structures and promotes interface-state formation, but the intrinsic nature of 2D germanene is preserved when the adlayer and substrate are fully incommensurate. This important consequence of adlayer-substrate commensurability is explained in light of competitive Ge-Ge and Ge-Ag bond formation. The physical mechanisms of film stability of the two phases will be discussed.

II. MATERIALS AND METHODS

A. Germanene growth

The germanene samples were prepared on a Ag(111) single crystal, with Ge evaporated from an effusion cell kept at 965 °C and with the substrate kept at 150 °C. The deposition rate is approximately 0.01 monolayer (ML) per minute. Here, 1 ML refers to the atom number of the Ag(111) layer. The silver crystal was cleaned by repeated sputter-anneal cycles and its cleanness was verified by sharp LEED diffraction spots and by direct STM imaging. We found that a slower Ge deposition rate and a moderately heated substrate facilitate better germanene growth, likely due to reduced random nucleation and enhanced Ge adatom mobility.

B. STM measurement

All STM data were taken at 77 K using a commercial Omicron low-temperature STM and flashed tungsten tips.

C. ARPES measurement

The angle-resolved photoemission spectra were measured with a Scienta R4000 energy analyzer and with *p*-polarized synchrotron radiation (27 and 35 eV) from the undulator beamline 21B1-U9 at the National Synchrotron Radiation Research Center in Taiwan and with unpolarized He-I light. The energy and angular resolutions were 10 meV and 0.3°, respectively.

D. Theoretical calculation

First-principles calculations were performed using the full-potential projected augmented wave method (PAW) [21,22] as implemented in the Vienna *Ab initio* Simulation Package (VASP) [23,24] with the Perdew-Burke-Ernzerhof (PBE)-type generalized gradient approximation (GGA) exchange-correlation energy functional [25] based on the density-functional theory (DFT). The supercell lattice structures of the striped phase (SP) and quasifreestanding phase (QP) observed in STM and LEED are optimized with a residue force less than 0.02 eV/Å. The self-consistent-field calculations are then performed with a cutoff energy of 300 eV over a 2 × 6 × 1 (or 2 × 2 × 1) Monkhorst-Pack *k*-point mesh in the 2D SBZ for the SP (or QP) phase. The total energies are converged to within 10^{-4} eV. To go beyond the standard GGA approach,

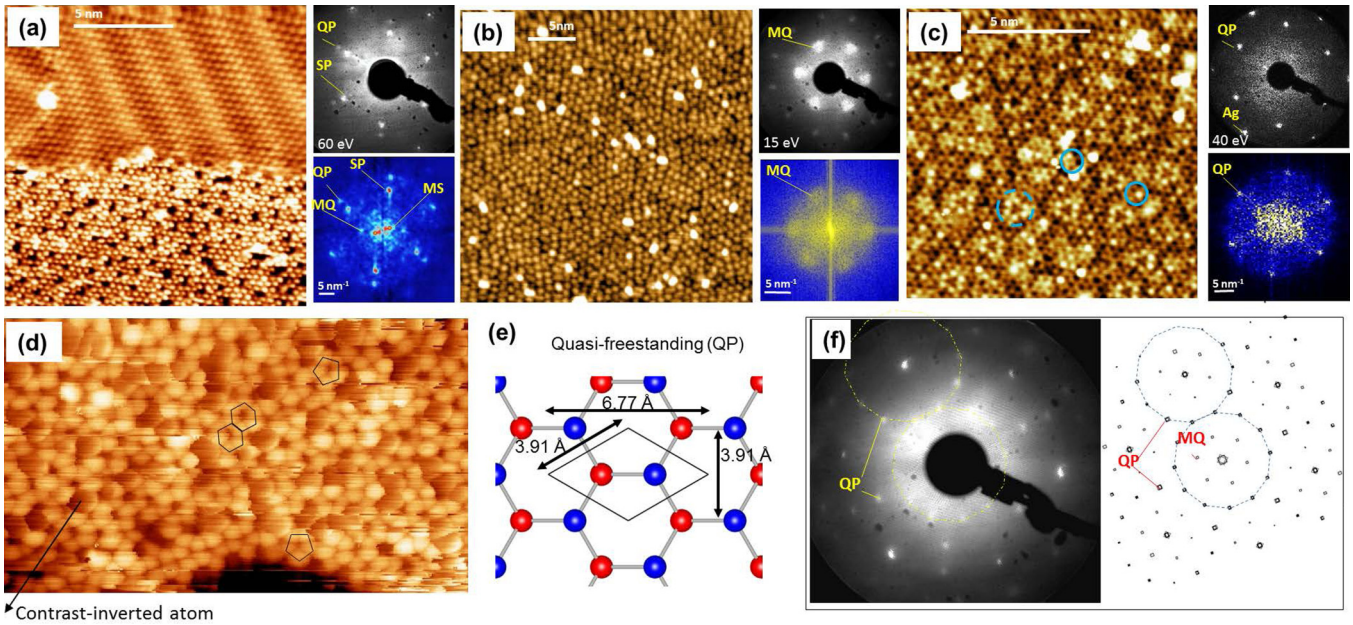

FIG. 2. "Quasifreestanding phase" germanene. (a) Coexisting SP and QP germanene (15 × 15 nm, −0.65 V, and 1.0 nA). (b) QP germanene shows a slightly disordered moiré pattern with a short periodicity ∼9 Å (30 × 30 nm, 1 V, and 1 nA). (c) Zoom-in micrograph of the moiré pattern shows adatoms (solid circles), local pinwheel-like structure (dashed circle), and a honeycomb lattice underneath: 11.6 × 11.6 nm, 0.1 V, and 0.73 nA. To the right of the (a), (b) topographic panels are the fast Fourier transform (FFT) images (blue) and LEED diffraction patterns (gray) of the respective phases. **SP**, **QP**, **MQ**, **MS**, **Ag**, respectively, denote the periodicities of SP germanene, QP germanene periodicity, QP "moiré," SP stripe, and Ag(111). Five-nm length scale bars, LEED beam energies, and FFT 5-nm^{-1} scales are noted in (a)–(c). See content for details. (d) Atom-resolved QP lattice (8 × 4.2 nm, 10 mV, and 0.73 nA). A honeycomb germanene lattice with slight disorder can be discerned. Imperfections (e.g., indicated Ge pentagon) are observed in the QP phase. Adatoms atop QP show inverted contrast with this imaging condition. (e) Proposed structure of the QP. (f) Simulation of the QP LEED pattern taken with 75-eV beam energy. See content for details.

we also perform calculations based on the more advanced Heyd-Scuseria-Ernzerhof (HSE) hybrid functional [26,27]. To compare with the ARPES results for SP, we unfold the band structures of the supercells to the first Brillouin zone of Ag(111) unit cell by using the BANDUP package [28]. The DFT constant energy contours (CECs) are calculated from the unfolded band structures of the SP with the Ag substrate. Because both the Ge and Ag are not heavy elements, we show only the results without spin-orbit-coupling (SOC) in the main text. Calculated results with SOC are shown in Figs. S6 to S8 in Supplemental Material [29].

The STM and LEED analyses shows that a 22 × 2 SP germanene supercell nearly matches the Ag(111) 30 × 2 supercell. To simulate the large superstructure observed in STM with reasonable correctness, we adopt a 6 × 2 germanene/8 × 2 Ag supercell in the calculations with 6 Ag(111) layers mimicking the substrate. This corresponds to a ratio of Ag close-packed distance vs germanene zigzag row width of 22/29.3, which is very close to the experimental ratio of 22/30. As discussed later in Fig. 1(a), the SP germanene endures strong tensile strains of, respectively, 23% and 12% along the $\mathbf{a}_1$**-zz** and **ac** directions as compared with freestanding germanene, with a buckling height of ∼0.1 Å. These tensile strain values are reproduced in the theory model (see Supplemental Material Table S1). Our total energy analysis demonstrates that the germanene at the hollow site of Ag(111) substrate is 0.06 eV/Ge [0.72 eV/supercell (6 Ge)] lower than the top site case. As shown in the Supplemental Material Fig. S6, the much simpler PBE + U scheme with $U = 4$ eV for Ag can reproduce the correct bulk Ag d band below −3.5 eV obtained by the more advanced hybrid HSE functional. Because the computational requirement of HSE is not reachable for the large SP supercell with Ag substrate, we use the much faster PBE + U method for the SP.

To simulate the incommensurate QP, we adopt a freestanding germanene 5 × 5 supercell with a 3.91-Å 1 × 1 unit-cell lattice constant as derived from our STM and LEED analyses and a buckling height of 0.93 Å. The larger buckling height accounts for the slight compressive strain in QP. These lattice parameters of 3.91 and 0.93 Å are slightly different from the DFT values of 4.06 and 0.75 Å of the freestanding germanene.

III. RESULTS

Ag(111) has been a prevalent choice for growing silicene, but it was reported to be unsuitable for germanene growth [16,17]. In contrast, our results support that germanene can grow on Ag(111) with proper growth conditions (see Materials and Methods section). At a Ge coverage of 1/3 ML, our STM and ARPES data are consistent with those of the $(\sqrt{3} \times \sqrt{3})R30^\circ$ Ag_2Ge alloy phase reported in the literature [12,30]. The band structure shows a Rashba-like feature at the Ag(111) $\bar{M}$ point. The embedded Ge atoms appear indistinguishable from the Ag substrate atoms in STM [12,30] but a dealloying process occurs at slightly higher Ge coverages (see Supplemental Material Figs. S1 and S3). The expelled Ag atoms appear to form islands near the substrate steps. Further

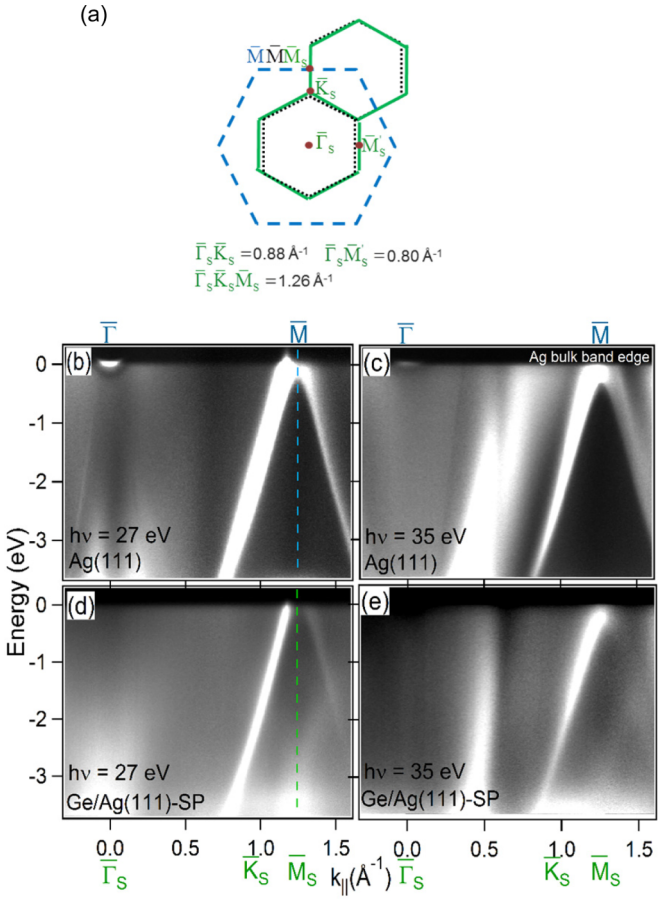

FIG. 3. Measured energy-band structures of SP germanene grown on Ag(111). (a) SBZs of Ag(111), Ag(111)-($\sqrt{3}\times\sqrt{3}$)$R30°$, and SP, marked by blue-dashed, black-dotted, and green-solid hexagons, respectively. The symmetry points are marked in the same color as the corresponding SBZs they belong to. (b)–(e) Measured energy-band dispersions of Ag(111), and SP germanene taken at the photon energies of 27 and 35 eV in the same symmetry direction marked by $\bar{\Gamma}-\bar{M}$ and $\bar{\Gamma}_S-\bar{K}_S-\bar{M}_S$, respectively, for their corresponding SBZs.

Ge deposition leads to the emergence of a new phase consisting of irregular striped features [see Supplemental Material Fig. S1(c)]. The stripes become better ordered with increasing Ge coverage. Eventually at about 0.74 ML, the system becomes a fully developed SP. A wide-area STM topographic scan [Fig. 1(c)] shows three striped domains oriented at 120° apart.

A detailed view of the SP [Fig. 1(a)] shows a low-buckled honeycomb pattern, which is modulated to form stripes. Each honeycomb hexagon consists of three up atoms interlaced by three down atoms with a STM height difference of ∼0.1 Å [Fig. 1(b) and inset]. A careful analysis of the SP pattern in relation to the underlying Ag(111) lattice reveals that the honeycomb lattice is uniaxially distorted. Along the germanene zigzag (**zz**) direction, which is also the $\mathbf{a}_1$ unit vector direction of the honeycomb lattice, the structure is commensurate with the Ag(111)-($\sqrt{3}\times\sqrt{3}$)$R30°$ (hereafter denoted as "$\sqrt{3}$-R30") unit cell; the honeycomb period is $\sqrt{3}$ times the Ag close-packed distance a_{Ag}. Along the perpendicular direction, or the germanene armchair (**ac**) direction, the SP lattice forms a modulated stripe appearance reminiscent of the herringbone reconstruction of Au(111) [31]. Closer inspection reveals that along **ac** the SP lattice is incommensurate with the Ag(111) and has a contracted lattice constant relative to the **zz** direction, but is still tensile strained with respect to freestanding germanene. The honeycomb lattice is continuous across the boundaries of orientation domains but the stripe pattern is sensitive to local strain caused by defects [see Supplemental Material Fig. S1(d)]. The stripe modulation is also evident from the slightly wavy atomic rows along the $\mathbf{a_2}$ and $\mathbf{a_3}$ directions [Fig. 1(a)]. LEED of this structure yields a rich pattern [Fig. 1(e)] consisting of clusters of diffraction spots. The seemingly complex pattern can be well modeled by multiple scattering [Fig. 1(f)] such that the momenta of diffracted electrons are sums of mixed crystal momenta of Ag(111) and germanene, similar to the LEED pattern of C_{60} on Ag(100) [32]. The LEED peak positions are at $\vec{k}=n_1\vec{G}_{\mathrm{stripe}}+n_2\vec{G}_{\mathrm{Ag(111)}}$ (n_1 and n_2 are integers). Simulated LEED patterns (see Supplemental Material Fig. S2), with different combinations of the silver lattice spacing (a_{Ag}) and the stripe phase periodicity (λ), give the closest agreement by matching 30 a_{Ag} to 22 germanene zigzag row widths along the **ac** direction. Consequently, SP germanene is highly tensile strained with respect to the freestanding germanene, with ∼23% strain along **zz** and ∼12% strain along **ac**, giving a Ge coverage of ∼0.74 ML. The derived unit cell of germanene (solid-line rhombus) and the $\sqrt{3}$-R30 unit cell (dashed-line rhombus) are shown in Fig. 1(d).

With additional Ge deposition, SP regions are converted into the QP starting at upper step edges [see Supplemental Material Fig. S1(d)]. It is an abrupt transition with no intermediate phases. Figure 2(a) shows a STM image over a region where the SP and QP coexist for a mixed sample, a LEED pattern (upper right), and a Fourier transform of the STM image (lower right). The spots labeled **QP**, **SP**, **MQ**, and **MS** correspond to the periodicities associated with the QP germanene honeycomb, SP germanene honeycomb, QP Moiré pattern, and SP moiré pattern, respectively. The **QP** spots, which bear resemblance to those of a bulk terminated Ge(111) surface, are not very sharp or intense but they nevertheless confirm the existence of certain long-range order. Figure 2(b) shows a fully converted QP sample in a larger view; the slightly disordered array of dots forms a clear ∼9-Å moiré modulation, which (feature **MQ**) can be seen in the Fourier transform of the STM picture and the LEED pattern. Figure 2(c) shows a zoom-in region, showing adatoms (solid circles), local pinwheel-like structure (dashed circle), and a honeycomb lattice underneath. In Fig. 2(d), with a tunneling gap resistance of ∼13 MΩ, a honeycomb lattice with some Ge atoms arranged in disordered pentagons or other nonhexagonal patterns can be identified. It is noted that different tunneling conditions emphasize different features in QP. The tunneling gap resistance used for the STM images shown in Figs. 2(b), 2(a), 2(c), and 2(d) decreases subsequently and different features such as moiré, buckled-up Ge atoms, barely atom-resolved QP, and atom-resolved QP are, respectively, enhanced corresponding to different gap resistance values.

The extracted lattice constant of 3.91 Å, as derived by the best-match LEED pattern [see Fig. 2(f) and Supplemental Material Fig. S2], leads to an incommensurate lattice with an ∼21% lattice shrinking from the closest commensurate $\sqrt{3}$-R30 cell. The lattice spacing of QP phase is rather close

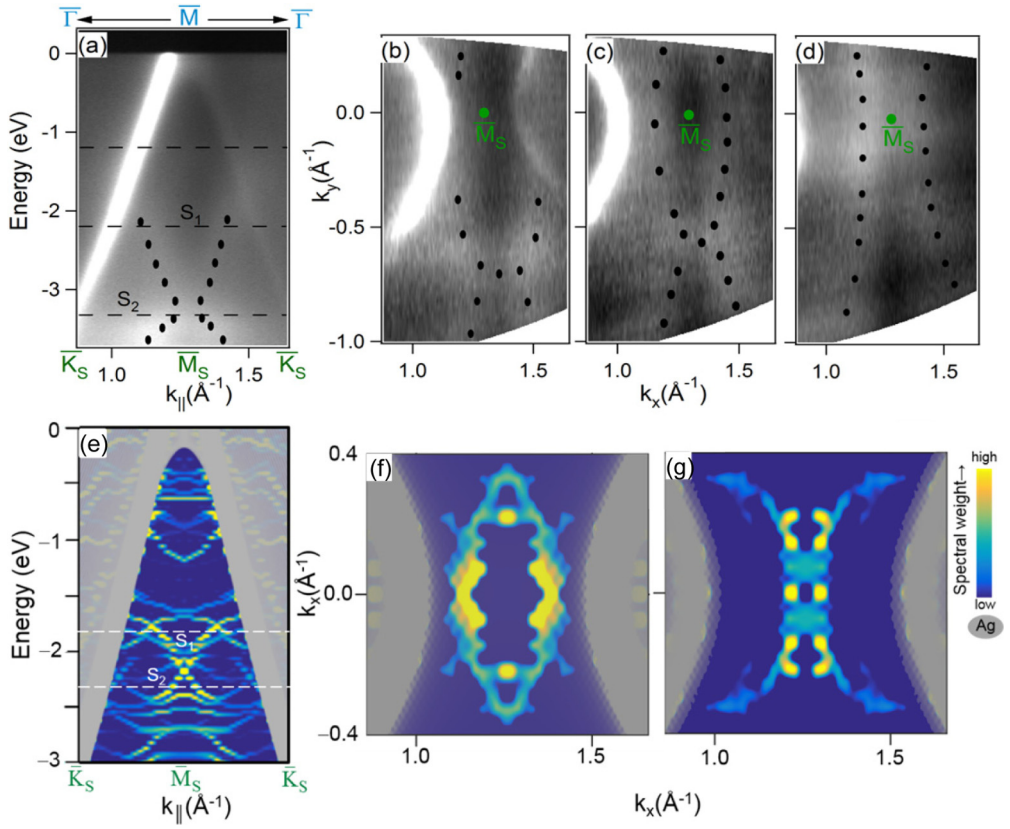

FIG. 4. Comparison between measured and calculated electronic structures for SP germanene. (a) Measured SP bands, S_1 and S_2, within the Ag bulk band gap centered at common $\bar{M}(\bar{M}_S)$. (b)–(d) Measured CECs at the energies of −1.2, −2.2, and −3.3 eV. (e) Calculated SP bands within the gap of Ag bulk projected bands (shaded gray area). (f), (g) Corresponding calculated CECs at the energies of −1.8 and −2.3 eV.

to the theoretical value of 4.06 Å for freestanding germanene [11], but with a slight compressive strain of ∼3.7% in the QP. The QP with a 3.91 Å Ge-Ge bond length gives a Ge coverage of 1.08 ML, about 45% higher than that of SP. This is consistent with the required Ge dosing time for full coverages of the SP and QP. Since both SP and QP are all single layers, the QP is therefore expected to be also a germanene honeycomb lattice. The QP unit cell is shown in Fig. 2(e).

The SP to QP structure phase transition causes a stronger lattice buckling in QP due to its ∼3.7% compressive strain with respect to an unstrained freestanding germanene. It also causes a significant 45% increase of areal Ge density in QP. The dramatic contraction of the QP lattice from the SP lattice could cause structure imperfection but further Ge deposition will partly repair these defects. Despite the partial local disorder in QP, this phase maintains a reasonable long-range order, as indicated by electron diffraction. Key electronic properties of germanene are expected to preserve even in a slightly defected QP; this is known in graphene and is confirmed for a defected QP model calculation [see Supplemental Material Fig. S8(f)].

Figure 3(a) shows the derived SBZs according to the SP lattice model in Fig. 1(d). Figures 3(b)–3(e) show the ARPES data taken with 27- and 35-eV photons for pristine Ag(111) and SP along $\bar{\Gamma}-\bar{M}$ of Ag(111) (equivalently, $\bar{\Gamma}_S-\bar{K}_S-\bar{M}_S$ of the SP). In the SP, the symmetry point $\bar{M}_S$ of the SP second SBZ and the $\bar{M}$ point of the Ag(111) first SBZ overlap in the commensurate **zz** direction but the SBZ sizes of the $\sqrt{3}$-R30 and SP differ by 12% in the incommensurate **ac** direction.

Results for pristine Ag(111) [Figs. 3(b) and 3(c)] show a Shockley surface state just below the Fermi level centered at $\bar{\Gamma}$ [33], a Λ-shaped projected Ag(111) bulk band edge centered at $\bar{M}$, and other band features. With Ge coverage, the Shockley surface state weakens but additional band features appear within the Λ-shaped bulk gap region. Such new features must be related to the germanene layer on the surface. In the SP [Figs. 3(d) and 3(e)], the surface state at $\bar{\Gamma}$ diminishes while a steep upward band starting at ~ -3.1 eV at $\bar{M}$ ($\bar{M}_s$) is evident. This new band is completely confined within the Ag bulk-projected gap, suggesting the formation of a Ge-induced interface-state band.

Figure 4(a) shows in detail the SP germanene-derived bands, which actually consist of the top S_1 and bottom S_2 (denoted by dots), around $\bar{M}_S$ along $\bar{K}_S-\bar{M}_S-\bar{K}_S$ [($\bar{\Gamma}-\bar{M}-\bar{\Gamma}$ of Ag(111)]. Figures 4(b)–4(d) display CECs around $\bar{M}_S$ at −1.2, −2.2, and −3.3 eV, respectively. The saddlelike intense features are derived from the Ag bulk band edge. Bands S_1 and S_2 are indicated by dots; the oval- and hyperbolic-shaped CECs exhibit weak dispersions along k_y ($\bar{\Gamma}_S-\bar{M}_S-\bar{\Gamma}_S$) because of the qausi-1D nature of these states associated with the stripe geometry. A comparison is made with theoretical ARPES maps [Figs. 4(e)–4(g)] using an approximating structure model (see the Materials and Methods section, and Supplemental Material Table S1 and Fig. S5 for details). Figure 4(e) shows the calculated supercell band structures unfolded back to the Ag(111) first SBZ, with the yellow color brightness indicating the weight of each band projected onto Ge atoms. A good

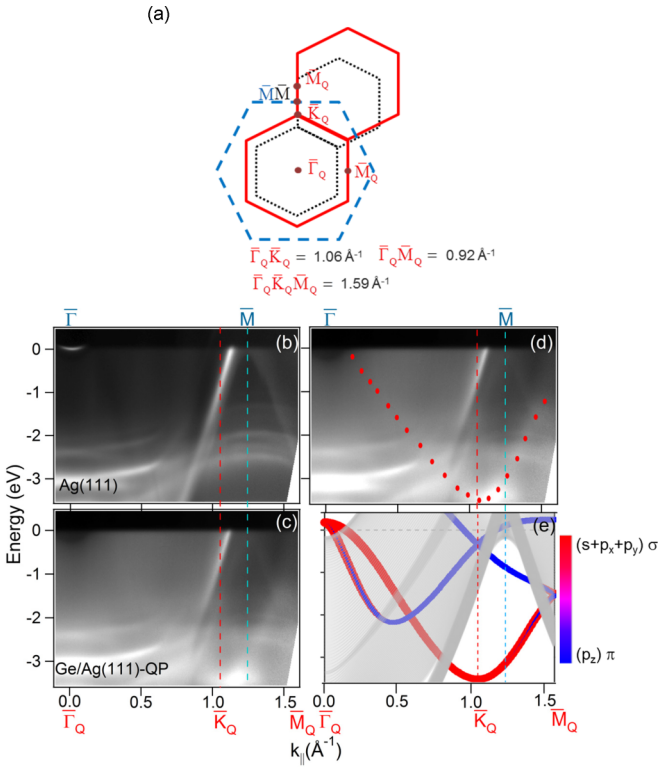

FIG. 5. Comparison between measured and calculated electronic structures for QP germanene. (a) SBZs of Ag(111), Ag(111)-$(\sqrt{3}\times\sqrt{3})R30^\circ$, and QP marked by blue-dashed, black-dotted, and red-solid hexagons, respectively. (b), (c) Measured energy-band dispersions of Ag(111), and QP germanene taken by He I UV light source in the same symmetry direction marked by $\bar{\Gamma}-\bar{M}$ and $\bar{\Gamma}_Q-\bar{K}_Q-\bar{M}_Q$. (d) The same figure as (c) with red dots superimposed to indicate QP band. (e) The calculated energy bands for a free-standing germanene superimposed with the Ag bulk band continuum (gray shade).

overall agreement between theory and experiment is evident except for an ∼0.9-eV offset with respect to the crossing point of S_1 and S_2 at $\bar{M}_s$ (see Supplemental Material Fig. S4). The calculated and measured CECs at an energy above the S_1 and S_2 crossing point [Figs. 4(f) and 4(b)], or below the crossing point [Figs. 4(g) and 4(d)] show agreeable elliptical or hyperbolic shapes sandwiched by the Ag bulk band edge. This agreement nicely supports the proposed structure model. Orbital character analysis, at the S_1 and S_2 crossing point at $\bar{M}_s$, shows that 51% are derived from Ag (26.4% sp and 24.8% d) and 49% from Ge (47.2% s, p_x, p_y, 1.2% p_z, and 0.3% d). This clearly indicates that the S_1 and S_2 bands are interface-state bands from the coupling of Ag surface and Ge adlayer.

As revealed by STM images in Figs. 2(c) and 2(d), the long-range ordered QP lattice still has some structure disorder. The energy band structures of QP are thus expected to be weaker and more difficult to observe. To enhance the possibility of observing QP-related energy bands, we used unpolarized He-I UV light, mainly He-I α with energy 21.2 eV, to conduct the ARPES measurement for QP in order to avoid the matrix-element selection rule in the dipole approximation. The SBZs derived from the lattice model in Fig. 2(e) are displayed in Fig. 5(a). Figure 5(b) shows the energy-band structure of pristine Ag(111). In addition to the Ag surface state at the surface zone center and Ag bulk band edge at the zone boundary, Ag d-band structures at $-2\sim-3$ eV are actually those excited by He-I β and γ,$h\nu = 23.09$ and 23.74 eV. At the coverage near QP germanene, one can observe from Fig. 5(c) a new energy band centered at $\bar{K}_Q$ (1.06 Å^{-1}) of QP at −3.5 eV rather than the symmetry point $\bar{M}$ of Ag(111). This band seemingly passes through the Ag bulk band continuum to Fermi level whereas the weak residue of SP interface band still remains. Most intensity weight of this energy band is concentrated on the region within the Ag band gap around $\bar{K}_Q$ and it smears out into Ag bulk band continuum.

A comparison between experiment and theory for the QP is presented in Figs. 5(d) and 5(e). We model the incommensurate QP by a freestanding germanene with a suitable buckling height [see Materials and Methods section and Supplemental Material Fig. S8(c)]. Figure 5(e) shows the computed germanene band structure (red and blue colors indicate the σ and π components) over the projected Ag bulk states (gray regions). The theoretical σ band agrees well with the observed band, as marked by the red dots in Fig. 5(d), on the overall momentum and energy positions of the band. The π bands, including Dirac cone near the Fermi level, are however not observed. The π electrons are mostly distributed above and below the honeycomb plane and are more likely than the in-plane σ electrons to hybridize with the Ag electrons to form partial bonding. This interaction could cause a substantial broadening of the π bands, rendering it too weak for ARPES observation. Similar behavior was also found for the (4×4) silicene grown on Ag(111) [5]. The partial bonding, being incommensurate, could lead to local structural disorder as observed by STM but it is also likely the source of stability for the formation of single-layer germanene instead of three-dimensional Ge crystallites.

Therefore, the QP electronic structure, although affected by the Ag substrate, retains some features of a freestanding germanene due to its incommensuration with the substrate.

IV. DISCUSSION AND CONCLUSION

The salient features of the SP and QP are in contrast. The SP is a very well ordered lattice but it does not show the intrinsic electronic structure of a freestanding germanene but instead an interface state. The QP has both long-range order and local disorder but it exhibits an electronic structure akin to that of freestanding germanene. Evidently the geometric structure of SP results from a compromise between the Ge-Ge tensile and the Ge-Ag interfacial strains, where the former (the latter) relaxes in the direction normal (parallel) to the stripe. The SP is stabilized through interfacial bonding along the commensurate direction (∼1 eV per Ge; see Supplemental Material Table S2). This bonding in turn generates the 1D-like S_1 and S_2 interfacial states within the Ag projected bulk band gap. Since this gap is significantly larger in Ag than the counterparts in Cu and Au, germanene formation on the Ag surface can be expected to be more favored than the other two cases. In the denser QP phase, Ge-Ge bonds relax to a freestanding germanene configuration at the cost of increased interfacial strain from the incommensurate Ge-Ag interfacial bonding. While this could cause more lattice disorder and imperfection, the intrinsic and

robust σ band of freestanding germanene is nonetheless better preserved, as shown in Fig. 5(c).

It was suggested that substrates enabling the 2D-Xene epitaxy should be commensurate with the freestanding 2D-Xene structure [20]. Our results of SP reveal that commensuration can renormalize the SP intrinsic electronic property from a freestanding germanene lattice, and germanene epitaxy does not necessarily require commensuration as indicated in the QP. The transformation from the tensile-strained SP to the denser QP illustrates a mechanism of triggering Ge-Ge bond relaxation to a freestanding configuration via additional Ge deposition. Such a mechanism is interesting and could also be achieved via deposition on SP by atoms species other than Ge.

In summary, evidence and salient features of dual phases associated with germanene are found by growing Ge on Ag(111), as supported by a detailed combined study of STM, ARPES, LEED, and *ab initio* theory. The basic structure is a low-buckled honeycomb lattice but because of the lattice mismatch with the substrate, the size of the honeycomb depends on the Ge coverage. At a lower Ge coverage, a partially commensurate SP forms. At a higher Ge coverage, a fully incommensurate QP forms. Evidently, Ag(111) provides a relatively gentle support for the formation and transformation of the dual germanene phases. Specifically, the SP is subjected to significant band renormalization and develops an interface state due to its partial commensuration with the substrate, whereas the QP reveals an electronic structure close to that of freestanding germanene because the incommensurate structure leads to a weaker and averaged-out interfacial interaction. Motivated by the idea of creating a real or nearly freestanding germanene, our work yields useful information toward this goal. Specifically, our results illustrate how the electronic and geometric structures correlate under incommensurate or partially commensurate conditions for Ge on Ag. The knowledge would be relevant to the science and technology for the fabrication of 2D honeycomb materials.

ACKNOWLEDGMENTS

We thank Ku-Ding Tsuei for arranging beam time in NSRRC. This research was supported by the Ministry of Science and Technology of Taiwan (Grant No. MOST 105-2112-M-007-017-MY3 to S.-J.T, Grant No. MOST 104-2112-M-002 -013 -MY3 to W.W.P., and Grant No. MOST 103-2112-M-007-018-MY3 to H.-T.J.) and by the US Department of Energy (Grant No. DE-FG02-07ER46383 to T.-C.C.). H.-T.J. acknowledges NCHC, CINC-NTU and NCTS, Taiwan, for technical support.

C.-H.L. and A.H. contributed equally to this work.

[1] K. S. Novoselov, A. K. Geim, S. V. Morozov, D. Jiang, Y. Zhang, S. V. Dubonos, I. V. Grigorieva, and A. A. Firsov, Electric field effect in atomically thin carbon films, Science **306**, 666 (2004).

[2] C. C. Liu, W. Feng, and Y. Yao, Quantum Spin Hall Effect in Silicene and Two-Dimensional Germanium, Phys. Rev. Lett. **107**, 076802 (2011).

[3] P. Vogt, P. De Padova, C. Quaresima, J. Avila, E. Frantzeskakis, M. C. Asensio, A. Resta, B. Ealet, and G. Le Lay, Silicene: Compelling Experimental Evidence for Graphenelike Two-Dimensional Silicon, Phys. Rev. Lett. **108**, 155501 (2012).

[4] C. L. Lin, R. Arafune, K. Kawahara, M. Kanno, N. Tsukahara, E. Minamitani, Y. Kim, M. Kawai, and N. Takagi, Substrate-Induced Symmetry Breaking in Silicene, Phys. Rev. Lett. **110**, 076801 (2013).

[5] S. K. Mahatha, P. Moras, V. Bellini, P. M. Sheverdyaeva, C. Struzzi, L. Petaccia, and C. Carbone, Silicene on Ag(111): A honeycomb lattice without Dirac bands, Phys. Rev. B **89**, 201416(R) (2014).

[6] G.-W. Lee, H.-D. Chen, and D.-S. Lin, Growth mode and structures of silicene on the Ag(111) surface, Appl. Surf. Sci. **354**, 187 (2015).

[7] P. De Padova *et al.*, The quasiparticle band dispersion in epitaxial multilayer silicene, J. Phys.: Condens. Matter **25**, 382202 (2013).

[8] J. E. Padilha and R. B. Pontes, Free-standing bilayer silicene: The effect of stacking order on the structural, electronic, and transport properties, J. Phys. Chem. C **119**, 3818 (2015).

[9] R. Yaokawa, T. Ohsuna, T. Morishita, Y. Hayasaka, M. J. Spencer, and H. Nakano, Monolayer-to-bilayer transformation of silicenes and their structural analysis, Nat. Commun. **7**, 10657 (2016).

[10] Y. Borensztein, A. Curcella, S. Royer, and G. Prévot, Silicene multilayers on Ag(111) display a cubic diamondlike structure and a $\sqrt{3} \times \sqrt{3}$ reconstruction induced by surfactant Ag atoms, Phys. Rev. B **92**, 155407 (2015).

[11] A. Acun *et al.*, Germanene: The germanium analogue of graphene, J. Phys.: Condens. Matter **27**, 443002 (2015).

[12] W. Wang, H. M. Sohail, J. R. Osiecki, and R. I. G. Uhrberg, Broken symmetry induced band splitting in the Ag_2Ge surface alloy on Ag(111), Phys. Rev. B **89**, 125410 (2014).

[13] P. Bampoulis, L. Zhang, A. Safaei, R. van Gastel, B. Poelsema, and H. J. Zandvliet, Germanene termination of Ge_2Pt crystals on Ge(110), J. Phys.: Condens. Matter **26**, 442001 (2014).

[14] L. Li, S. Z. Lu, J. Pan, Z. Qin, Y. Q. Wang, Y. Wang, G. Y. Cao, S. Du, and H. J. Gao, Buckled germanene formation on Pt(111), Adv. Mater. **26**, 4820 (2014).

[15] M. Derivaz, D. Dentel, R. Stephan, M. C. Hanf, A. Mehdaoui, P. Sonnet, and C. Pirri, Continuous germanene layer on Al(111), Nano Lett. **15**, 2510 (2015).

[16] M. E. Dávila, L. Xian, S. Cahangirov, A. Rubio, and G. Le Lay, Germanene: A novel two-dimensional germanium allotrope akin to graphene and silicene, New. J. Phys. **16**, 095002 (2014).

[17] M. E. Davila and G. Le Lay, Few layer epitaxial germanene: A novel two-dimensional Dirac material, Sci. Rep. **6**, 20714 (2016).

[18] L. Zhang, P. Bampoulis, A. N. Rudenko, Q. Yao, A. van Houselt, B. Poelsema, M. I. Katsnelson, and H. J. Zandvliet, Structural and Electronic Properties of Germanene on MoS_2, Phys. Rev. Lett. **116**, 256804 (2016).

[19] F. F. Zhu, W. J. Chen, Y. Xu, C. L. Gao, D. D. Guan, C. H. Liu, D. Qian, S. C. Zhang, and J. F. Jia, Epitaxial growth of two-dimensional stanene, Nat. Mater. **14**, 1020 (2015).

[20] A. Molle, J. Goldberger, M. Houssa, Y. Xu, S. C. Zhang, and D. Akinwande, Buckled two-dimensional Xene sheets, Nat. Mater. **16**, 163 (2017).

[21] P. E. Blöchl, Projector augmented-wave method, Phys. Rev. B **50**, 17953 (1994).

[22] G. Kresse and D. Joubert, From ultrasoft pseudopotentials to the projector augmented-wave method, Phys. Rev. B **59**, 1758 (1999).

[23] G. Kresse and J. Furthmuller, Efficient iterative schemes for *ab initio* total-energy calculations using a plane-wave basis set, Phys. Rev. B **54**, 11169 (1996).

[24] G. Kresse and J. Hafner, *Ab initio* molecular dynamics for open-shell transition metals, Phys. Rev. B **48**, 13115 (1993).

[25] J. P. Perdew, K. Burke, and M. Ernzerhof, Generalized Gradient Approximation Made Simple, Phys. Rev. Lett. **77**, 3865 (1996).

[26] J. Heyd, G. E. Scuseria, and M. Ernzerhof, Hybrid functionals based on a screened Coulomb potential, J. Phys. Chem. **118**, 8207 (2003).

[27] J. Heyd, G. E. Scuseria, and M. Ernzerhof, Erratum: "Hybrid functionals based on a screened Coulomb potential" [J. Chem. Phys. **118**, 8207 (2003)], J. Phys. Chem. **124**, 219906 (2006).

[28] P. V. C. Medeiros, S. Stafström, and J. Björk, Effects of extrinsic and intrinsic perturbations on the electronic structure of graphene: Retaining an effective primitive cell band structure by band unfolding, Phys. Rev. B **89**, 041407 (2014).

[29] See Supplemental Material at http://link.aps.org/supplemental/10.1103/PhysRevMaterials.2.024003 for comparison.

[30] H. Oughaddou, S. Sawaya, J. Goniakowski, B. Aufray, G. Le Lay, J. M. Gay, G. Treglia, J. P. Biberian, N. Barrett, C. Guillot, A. Mayne, and G. Dujardin, Ge/Ag(111) semiconductor-on-metal growth: Formation of an Ag_2Ge surface alloy, Phys. Rev. B **62**, 16653 (2000).

[31] S. Narasimhan and D. Vanderbilt, Elastic Stress Domains and the Herringbone Reconstruction on Au(111), Phys. Rev. Lett. **69**, 1564 (1992).

[32] C.-L. Hsu and W. W. Pai, Aperiodic incommensurate phase of a C60 monolayer on Ag(100), Phys. Rev. B **68**, 245414 (2003).

[33] G. Nicolay, F. Reinert, S. Hüfner, and P. Blaha, Spin-orbit splitting of the *L*-gap surface state on Au(111) and Ag(111), Phys. Rev. B **65**, 033407 (2001).